This is a repository copy of *Oscillating flames in open tubes*.

White Rose Research Online URL for this paper:
http://eprints.whiterose.ac.uk/90868/

Version: Accepted Version

1. Title: Oscillating flames in open tubes

2. Authors and affiliations: Yang J[a], Mossa F. M. S[a], Huang H. W[a], Wang Q[b], Woolley R[a](✉), Zhang Y[a]

[a] Department of Mechanical Engineering, the University of Sheffield, Sheffield, S1 3JD, UK

[b] School of Mechanical Engineering, Shanghai Jiao Tong University, Shanghai, 200240, China

3. Corresponding author's contact information:
Mailing address:

The University of Sheffield

Department of Mechanical Engineering

Mappin Street

Sheffield

S1 3JD

UK

Email: Rob.Woolley@sheffield.ac.uk

Phone: +44 114 2227711
Fax: +44 114 2227711

4. Colloquium: Detonations, Explosion, and Supersonic Combustion

5. Total length of paper and method of determination

Total length: 6173 words

Method of determination: Method 1

6. List of word equivalent lengths

Items	Equivalent lengths
Main text	3846
References	326
Equations	46
Figure 1 with caption	191
Figure 2 with caption	363
Figure 3 with caption	174
Figure 4 with caption	77
Figure 5 with caption	767
Figure 6 with caption	249
Figure 7 with caption	134
Total	**6173**

Oscillating flames in open tubes

Yang J[a], Mossa F. M. S[a], Huang H. W[a], Wang Q[b], Woolley R[a]([⧈]), Zhang Y[a]

[a] *Department of Mechanical Engineering, the University of Sheffield, Sheffield, S1 3JD, UK*
[b] *School of Mechanical Engineering, Shanghai Jiao Tong University, Shanghai, 200240, China*

Email: Rob.Woolley@sheffield .ac.uk

Phone: +44 114 2227711
Fax: +44 114 2227711

Abstract

When a flame passes along a tube that is open at both ends a self induced fluctuating pressure/flow field is created which the flame has to traverse. Here fuel rich ($1.1 < \phi < 1.4$) propane-air flames have been filmed travelling along a 20 mm internal diameter quartz tube. Fluctuations in the flame's progression were observed to increase as the flame propagated, achieving maximum oscillation amplitude of ± 10 mm at 220 Hz that decayed as the flame progressed further towards the end of the tube. The impact of the periodic pressure gradients on the flame shape could be discerned with tongues of unburned reactants pushed into the products as well as the corresponding rapid acceleration of the flame into the unburned mixture. The impact of the fluctuations on flame chemistry was monitored by capturing the CH* and C_2* chemiluminescence using a high speed colour camera. The CH*/C_2* was observed to decrease as the flame was pulled back towards the burned mixture; and increased when the the flame was pushed forwards. This was consistent throughout the flame progress even when small oscillations in the flame position were measured. This could be a significant feature of flames in this environment.

Keywords: Unsteady flames, Acoustic Oscillations, High speed imaging, DFCD image processing, Chemiluminescence

1. Introduction

The transition from an ignition to detonation remains a challenging problem in combustion science. The initial deflagration must accelerate sufficiently that a detonation wave is formed. A number of different mechanisms have been suggested that may be involved in this process: cellular flames resulting from laminar instabilities, obstacles creating turbulent flames, flame shock-wave interactions, and acoustic flame instabilities [1]. The last of these, acoustic flame instabilities, have been observed in tubes and are thought to be of significance in spaces that are free of obstructions [1].

The investigation of the propagation of flames in tubes dates back to the beginning of combustion science with the pioneering studies of Mallard and Le Chatelier [2]. Experiments on flames in tubes continued throughout the twentieth century. Notable examples are:

(i)   The measurements performed in Sheffield in the 1920's and 1930's initiated by Richard Vernon Wheeler where high-speed imaging was used to capture the flame movement [3]. This work was pursued for its relevance to mine gas explosions and culminated in measurements of the laminar burning velocity, later refined by Gerstein et al. at the Lewis Flight Propulsion Laboratories [4].

(ii)   Guénoche performed further experimental studies examining a range of phenomena within tubes to better understand non-steady flame propagation [5].

This apparently simple geometry demonstrates complex behaviour that changes with tube diameter, boundary conditions (e.g. open or closed ends) and the fuel-air properties. Flames progress both steadily and are subject to violent vibrations. In the case of oscillating flames, the

flame front can become distorted and wave amplification may occur caused by the coherence between the acoustic wave and heat release [1]. The problem is important for understanding flame acceleration, flame hazards and also miniaturised combustion devices. Recently, research has concentrated on numeric solutions to this problem typically with simplified chemistry. For example, flame oscillation has been demonstrated in tubes with open ends and no slip walls, the trigger being the increasing flame surface area resulting from interaction with the walls [6].

Here propane-air flames propagating along a tube have been imaged with high speed cameras and the measurements reported. The ends of the tube were open and in some circumstances a fluctuating pressure/velocity field was generated in the central length of the tube that the flame had to traverse. The action of the waves on the propagating flame was observed and also the chemiluminescence of the flames analysed.

For hydrocarbon flames, the visible emanating energy can be attributed to the spectra of electronically excited combustion radicals CH* (430nm) and C_2* (Swan system, dominant emissive band heads at 473.71 nm and 516.52 nm), and the continuous spectrum from solid carbon/soot [7]. The intensity of the energy released by these spectra is related to a number of factors such as the burning condition, fuel and fuel-to-oxidizer ratio, which consequently affect the colour perceived from a flame. Thus, the colour of a flame can be used to provide information on its generic spectrometric composition through careful calibration.

The use of the emission of excited combustion radicals to determine information about flames (e.g the heat release rate and equivalence ratio) dates back to the 1950's, for example see [8]. Initially the signal of an individual excited species was gathered, however, in recent years the ratio of two species has been found to be a useful parameter for the measure of equivalence ratio [9]. The ratio of CH*/OH* has been used in the majority of reported experiments [10]; as it lends itself to measurement using photomultipliers (and spectrometers) and chemical kinetic modelling is

feasible. The signal is strongly modified by quenching where a non-reactive molecule collides with an excited molecule absorbing its excess energy this is a function of both the temperature and pressure [7]. The local stretch rate and curvature may also influence the emission by excited species [10, 11]. In this study, high-speed flame imaging was utilised and the CH^*/C_2^* is obtained as the camera and associated optics could not detect UV light and hence OH^*. The emission from both CH^* and C_2^* were captured simultaneously onto the same detector and image processing used to separate the signals. The CH^*/C_2^* ratio has been shown have a linear response to equivalence ration [12].

Modern digital high-speed colour cameras encodes the captured visible radiation into three discrete signal ranges with sensitivity peaking in the R, G and B portion of the visible electromagnetic spectrum. In this form, digital colour cameras can be considered as a device that offers limited multi-spectral discrimination in addition to its spatial functionality. Based on this, a DFCD (Digital Flame Colour Discrimination) combustion quantification scheme has been created by Huang et al. [13]. The DFCD approach has already been successfully applied in the characterisation of diffusion and premixed hydrocarbon flames; providing the trends of spectroscopic-derived CH^* and C_2^* emission distributions over range of equivalence ratios [14], and the local fuel/air mixture [15].

As the flames studied here were inherently 3D, a stereo adapter was also mounted onto the camera lens, this permitted the recovery of depth that, with appropriate post processing, would allow the flame to be visualised in 3D.

2. Experimental setup

Propane-air flames were ignited at one end of a 1200 mm long horizontal tube of 20 mm internal diameter with both ends open to atmosphere. A schematic of the rig was shown in Fig 1(a). It consisted of two connected parallel pipes, using two three way valves the rig can be arranged in

two configurations. For filling, the pipes are connected together in a loop, Fig. 1(b); fans are used to mix the fuel and air which were injected into the rig after the previous combustion products had been evacuated. The mixed fuel/air mixture was ignited down a straight tube and the flame filmed in configuration, Fig 1(c). Typically, five measurements were performed at each condition. The initial temperature was that of the lab, typically 293K. Experiments were performed across the ignitable range of equivalence ratios. The central section of the tube was quartz to enable the flame to be visualised. The flame propagation was tracked using a variety of high speed cameras: a Casio EX-FH100 framing at 420 fps; a monochrome Photosonics Phantom v210 framing at 3000 fps with a shutter speed of 332 μs; and a Photron SA-4 colour camera coupled with a Sigma EX DG 24-70 mm, f-2.8 zoom lens, framing rate 1000 fps and 1000 μs.

Ignition was performed using a pilot flame. This was achieved by opening a port at one end of the tube and directing a flame from a gas lighter into the tube. The propagation of flames in tubes was found to vary considerably with the ignition source. Spark ignition has been found to enhance the onset of flame oscillations and so was not used here. The tube was mounted horizontally to minimize gravitational effects as upwardly propagation flames have been shown to propagate faster than downward moving flames with differences in flame shape [16].

In the case of the 1000 fps colour filming, an Asahi Pentax (two inner and outer mirrors) stereo-adapter was mounted onto the lens of the camera. The stereo adapter was perpendicular to the camera body and the stereo images appeared in the top and bottom of the recorded image. In this configuration, the stereo-adapter directs the incident rays from the scene onto the image plane from two different view angles through the mirrors. Further details of the stereoscopic imaging configuration can been found in Ng and Zhang [17]. The flame then can be visualised in 3D though the NVIDIA 3D Vision viewer software.

The colour images were processed to provide CH* and C_2* emission levels. Only the top side of the image pairs was processed via the DFCD in Matlab. The DFCD is based on the characterisation of the colour signal emanating from the flame [13]. Based on the previous investigations, suitable ranges of Hue (H), for signifying the different flame colour appearance, have been identified using varying hydrocarbon fuel compositions [13, 14 and 18]. The spectral sensitivity response of CCD/CMOS sensors varies across the spectrum of visible wavelengths. Thus, the characteristic flame colour fidelity induced by known visible intermediate radicals such as the CH* and the C_2* are confined to discrete ranges of occurrences in both the *RGB* and the *H* of the *HSV* colour space. By taking into account pixel populations with *P(i, j)* conformity, the relative trends of CH* and C_2* chemiluminescence intensity variations obtained through spectrometry along with changes in ϕ can be modelled [14].These signatures have been applied to digital images and the perceived visible premixed flame colour variations were found to be consistent within two discrete ranges of:

$$P(i,j) \approx 120° < H < 240° \tag{1}$$

where *P(i, j)* denotes pixel populations with premixed flame like bluish flame colorations. The CH*/C_2* ratio of two radical chemiluminescence intensities have been previously used to provide indications of the global fuel/air mixture state of a premixed flame [19]. The blue and green emissions (in the RGB colour space) were found to model well with the CH* and C_2* chemiluminescence intensities, respectively. Similarly, in this investigation a B/G colour signal ratio profile was employed in the form of:

$$(B/G) \in P(i,j) \tag{2}$$

The evaluation for a range of equivalence ratios was performed on a burner with an inner nozzle diameter of 10 mm to examine premixed C_3H_8 flames from ϕ = 0.97 to 1.81. Fourteen cases were examined at constant fuel flow rate of 110 mL/min and the premixing air flow rate altered from 1.5 to 2.8 L/min. For each case, 1500 image frames were acquired at 125 fps. Shown in Fig. 2a is a

typical histogram of the computed *B/G* values. These distributions are then fitted using an assumed

Gaussian distribution to calculate the characteristic mean and variance (μ_e and σ^2 respectively) at

different conditions. Computed Gaussian distributions are shown in Fig. 2b of the $(B/G) \in P(i,j)$

population. Discrete μ_e peaks are illustrated from $\phi = 0.97$ to 1.60. Between $\phi = 1.60$ and 1.81, the

level of $(B/G) \in P(i,j)$ ratio remained consistent along with increase in ϕ.

The observed discrete variation of the μ_e values suggests that a curve fitting algorithm may be

applied to compute the corresponding ϕ state based on the calculated μ_e of the colour ratio

distribution. It is however evident from Fig 2b, that the broadness of the distribution means that

an additional step needs to be taken to evaluate the accuracy of μ_e. The resultant μ_e and its

prediction range between $\phi = 0.97$ and 1.60 is shown in Fig. 3. As it can be seen even at 99% *CI*

(confidence interval), the variation of the computed μ_e is small; the upper and lower limits are

typically less than 1% from each characteristic μ_e at different ϕ. Therefore, despite the observed

broadness of the Gaussian distributions seen in Fig. 2b, the actual fluctuation of μ_e is small. The

Gaussian mean from the spatial $(B/G) \in P(i,j)$ population may be considered as discrete and a

sixth order polynomial curve-fitting applied to calculate the ϕ_e from the population with conformity

to Eq. 2. Importantly, this provides a correlation to evaluate the spectral flame colour fidelity

observed from the ignition-to-combustion event and its association with ϕ under conditions

considered in this study.

3. Results

Flames were imaged over the ignitable range of equivalence ratios. At both the leanest and richest

values of ϕ the flame propagated steadily, however from $1.1 < \phi < 1.4$ the flame was subjected to

fluctuations in the central part of the tube. For ϕ of 0.8, 0.9 and 1.0, shown in Fig. 4, observed

steady flame speeds of 1.3, 1.9 and 2.3 m/s were measured. These are significantly higher than the

measured laminar burning velocities of 0.27, 0.35 and 0.38 m/s for these ϕ.. These are typical of

flames observed in tubes, where the flame is convex relative to burned gases, and slightly tipped forwards [5]. The overall flame shape is the result of the no slip condition at the walls acting (primarily) on the burned gases in addition to heat transfer from the reaction zone to the wall. The tipping is thought to occur due to the hot and less dense combustion gases behind the flame rising relative to the cooler unburned mixture and is most evident in the flame with the lowest burned gas density. However, asymmetrical flame shapes have also been observed in upwardly propagating flames and the initial development of the flame following ignition may be of significance [5].

At richer mixtures a transition occurs where a oscillatory (vibrational) behaviour was observed. These flames will be the primary subject of this paper. To resolve the progress of these flames, framing rates of 3000 fps were used. Images of one these flames at two different positions in the tube are shown in Fig. 5. Flame position and propagation were characterised using the leading point of the flame. The ignition was performed out-of-sight of the camera with a pilot flame and its occurrence was not monitored. This meant it was not straightforward to define a consistent time zero and the times used here relate to when the camera was triggered rather than any specific event. Times are used in the text to reference particular frames in the image sequences. The flame position in the tube plotted against time is shown in Fig 6, for the flame in Fig 5.

To determine the magnitude of the oscillations separately from the distance of flame travel, a low pass fft filter was applied to the data in Fig 6(a). The deviation from the filtered flame position is shown in Fig. 6(b). From this it can be seen that oscillations were present throughout the time that the flame was recorded. Their amplitude increasing until they achieved a maximum of ±10 mm from the filtered flame position. Then, the oscillations declined rapidly. The frequency of the oscillations throughout the first 100 ms was found to be 220 Hz; similar values were obtained for all unstable flames in the range $1.1 < \phi < 1.4$. Shown in Fig. 6(c) is the flame speed derived from the

filtered flame position data. The mean velocity initially was initially constant (albeit with small fluctuations in position and hence velocity), it then decelerated to a velocity of ~1.6 m/s before accelerating and reaching a peak mean flame speed ~4.9 m/s corresponding with the maximum oscillation. From that point on the velocity rapidly decays to ~0.9 m/s, similar to that observed at the beginning of the tube. The peak velocities are approximately 10 times higher than quoted values of the laminar burning velocity.

The flames subjected to the oscillations were found to be repeatable. This was determined by monitoring the frequency and amplitude of the oscillations in flame position as shown in Fig. 6(b). For a sample of 10 experiments for ϕ = 1.1 to 1.3, the frequency was found to be 227 Hz (Standard deviation 6Hz) and the maximum in oscillation amplitude ± 12.1 mm (Standard deviation 1.2 mm). Thus, once the acoustic field was created the differences in flame properties were found to have no further influence. This justifies the detailed reporting of only two events in this manuscript.

Sequences of the flame propagation are shown in Fig. 5. The first series (A) of high speed images shown are for the flame at 38 ms. Here, relatively slight oscillation in the flame position could be detected with the flame front moving approximate ± 2 mm about the filtered position. In the first 6 frames (38 – 39.6 ms) the flame front was stationary. In that time the length of the flame, i.e. the distance from the convex front of the flame in the central part of the tube diameter to the back where it is situated close to the tube walls, decreases. In the latter part of the sequence, the back of the flame remains stationary but the front of the flame moves forward. Both the flame area and shape are thus constantly changing throughout the propagation. A zoological analogy of such movement might be a caterpillar that begins each crawl by a step of the insect's rear legs followed by a forward moving wave of steps by its middle legs.

The second sequence of images (B) is taken around 89 ms and corresponds to the maximum flame velocity and oscillation of the flame. Here the amplitude of the oscillation was found to be ± 10 mm

relative to the filtered position. In the first frame of the sequence (88 ms), the front of the flame is approximately planar. However there exists a long tail into the burned gas which suggests the occurrence of a Rayleigh-Taylor instability induced by a pressure gradient travelling from the unburned to burned gases [20]. For the first seven images in the sequence the whole flame was pulled backwards in the direction of the burned gases. This occurs preferentially at the walls. The flame grows forward from 98.6 ms onwards along the centre of the tube almost as a spherical ball progressing outwards from the middle of the flame 'brush'. The front edge of this growth is initially dim and diffuse but becomes brighter and sharper. As this front slows the front of the flame flattens. Whilst the flame propagates forwards it is also being pulled backwards into the burned gases at the walls. Thus, the flame is only travelling forward for one half of the oscillation. Animations of the direct flame imaging are provided in the Supplementary Material.

High speed colour images were also captured of these oscillating flames (although for a different event and at lower framing rate). The CH^* and C_2^* luminescence were identified and the ratio obtained. The value of CH^*/C_2^* would be expected to remain constant as the unburned gases are fully mixed. Maps were obtained at similar positions in the pipe as Fig. 5 A and B and these are shown in Fig. 5 C and D. The times refer to the camera setting and their absolute value is not significant. Noticeable changes in CH^*/C_2^* can be observed. As the flame was drawn back towards the burned gases the CH^*/C_2^* fell, potentially indicating a modification of the reaction mechanism at the flame front. This is particularly apparent between 52 and 55 ms in Fig. 5 D. Shown in Fig. 7 is CH^*/C_2^* plotted against time from ignition and the flame position. Changes in the CH^*/C_2^* ratio can be seen throughout. The amplitude of the fluctuations in CH^*/C_2^* increased only slightly whilst the flame was filmed. From the flame front position curve it can be seem that oscillations were present throughout the filming. The flame front position is out of phase with CH^*/C_2^*, as the flame moves back towards the burned gases CH^*/C_2^* increases and vice versa. Animations of the CH^*/C_2^* processed images are provided in the Supplementary Material.

Any statement concerning CH^*/C_2^* must be tempered as the pressure and hence magnitude of quenching are not known. The quenching of both CH^* and C_2^* are likely to significantly alter with the pressure [9], although measurements of CH^*/OH^* demonstrate little difference up to 3 bar [10]. The authors are not aware of measurements examining the influence of pressure on CH^*/C_2^*. The acoustically induced pressure waves are likely to be relatively small (typical values are ±1000 Pa [21]) as both ends of the tube are open. In Fig. 7 changes in CH^*/C_2^* can be observed at the early stages of induced oscillation where the magnitude of the pressure variation can be assumed to be small.

The propagation of flames in tubes has received some interest in recent years as a modelling study. Much of the behaviour seen here is described in these studies. One dimensional analysis has been performed for a ignition at a closed end for the flame propagating towards the open end [22]. Tube acoustics are set in motion and oscillations in the front position are strong enough to result in flow reversal. A dramatic increase in the propagation speed and Rayleigh–Taylor instability were observed. Cui et al. have modelled a flame subjected to alternating flows that both support and oppose the flame [23] for different boundary conditions. For large Lewis number flames (not the case in this experimental work) they found that the flame created a pulsating mode and that it was subject to short intervals of vigorous burning followed longer intervals where burning intensity was low. Violent flame folding has been observed in models of flame-acoustic resonance for a flame travelling from an open end to a closed end [24]. The Rayleigh-Taylor instability was observed and the formation of 'blobs' of burnt matter being pushed into the fuel-air mixture. Akkerman et al. [6] have examined the problem of open-ended tubes and demonstrated a self induced flame oscillation where the flame performs a concave to convex transition with an acceleration of the flame associated with its convex shape.

4. Conclusions

When flame a passes along a tube that is open at both ends a self induced fluctuating pressure/flow field is created which the flame has to traverse. Here fuel rich ($1.1 < \phi < 1.4$) propane-air flames have been filmed travelling along a 20 mm internal diameter quartz tube. Fluctuations in the flame progress were observed to increase as the flame propagated achieving a maximum oscillation amplitude of ± 10 mm at 220 Hz which then decayed as the flame progressed towards the end of the tube.

For small fluctuations (oscillation amplitude ± 1 mm) the flame was observed to propagate with caterpillar-like movement along the tube; where the back of the flame nearest to the tube remained anchored and the front moved forward and then the front of the flame remained stationary and the back moved forward. As the oscillations increased dramatic changes in the flame shape could be discerned with tongues of unburned reactants pushed into the products as well as rapid accelerations of the flame into the unburned mixture. At the point of maximum oscillation, the unfiltered flame speed achieved ~4.9 m/s, twice the speed of the flame when the fluctuations were small, and that is an order of magnitude higher than the laminar burning velocity.

The impact of the pressure fluctuations on the flame chemistry was monitored by capturing the CH^* and C_2^* chemiluminescence using a high speed colour camera, with the object to monitor changes in flame chemistry as the flame traversed the fluctuating pressure field. The CH^*/C_2^* ratio was observed to decrease as the flame was pulled back towards the burned mixture. It then increased as the flame moved forward. This was seen throughout the flame progress even when oscillations in the flame position were small. Further work is required to correlate to CH^*/C_2^* to the local burnrate and to determine the effect (if any) of quenching on the chemiluminescence signal due to pressure variations. Observation of the maps of CH^*/C_2^* might indicate that in this case the higher its value the 'better' the local burn; these are fuel rich flames and higher values CH^*/C_2^* are

typical of leaner ϕ. Further work would be required to confirm this. Variations in the local equivalence ratio are thought unlikely as the unburned gases were well mixed.

References

[1] G. Ciccarelli, S. Dorofeev. Prog. Energy Combust. Sci. 34 (2008) 499–550.

[2] E. Mallard, H. L. Chatelier, Ann. Mines 8 (4) (1883) 274.

[3] H. F. Coward, F. J. Hartwell, J. Chem. Soc. 1996 (1932) 2676-2684.

[4] M. Gerstein, O. Levine, E. L. Wong. America Chemi. Soci. 73 (1) (1951) 418-422.

[5] H. Guénoche. Pergamon, New York (1964) 107-160.

[6] V. Akkerman, C. K. Law, V. Bychkov, L. K. Eriksson. Physics of Fluids 22 (2010) 053606.

[7] A. G. Gaydon. The Spectroscopy of Flames. London: Chapman and Hall (1974).

[8] T. Clark. NACA Technical Note (1958) 4266.

[9] B. Higgins, M. Q. McQuay, F. Lacas, J. C. Rolon, N. Darabiha, S. Candel. Fuel 80 (2001) 67-74.

[10] T. M. Muruganandam, B. H. Kim, M. R. Morrell, V. Nori, M. Patel, B. W. Romig, J. M. Seitzman. Proc. Comb. Ins. 30 (2005) 1601–1609.

[11] H. N. Najm, P. H. Paul, C. J. Mueller, P.S. Wyckoff. Combust. Flame 113 (3) (1998) 312-332.

[12] L. C. Haber. Virginia Polytechnic Institute and State University. MSc Thesis, (2000).

[13] H. W. Huang, Y. Zhang. Meas. Sci. Technol. 19 (8) (2008) 085406.

[14] H. W. Huang, Y. Zhang. Fuel 90 (2010) 48-53.

[15] H. W. Huang, J. Yang, Q. Wang, Y. Zhang. Fuel 103 (2013) 334-346.

[16] A. Hamins, M. Heitor, P. A. Libby. Acta Astronautica 17 (5) (1988) 503-514.

[17] W. B. Ng, Y. Zhang. Experiments in Fluids 34 (2003) 484-493.

[18] H. W. Huang, Y. Zhang. Meas. Sci. Technol. 21 (2010) 085202.

[19] J. Kojima, Y. Ikeda, Nakajima. Combust. Flame 140 (2005) 34-45.

[20] A. C. McIntosh. LNP 449 (1995) 176-192.

[21] C. Jiménez, J. Quinard, J. Graña-Otero, H. Schmidt, G. Searby, Combust. Flame 159 (2012) 1894-1908.

[22] C. Regis L. Bauwens, Luc Bauwens, Ida Wierzba, Proc. Comb. Ins. 31 (2007) 2381–2388

[23] C. Cui, M. Moshe, T. L. Jackson. AIAA 43 (6) (2005) 1284-1292.

[24] A. Petchenko, V. Bychkov, V. Akkerman, L.E. Eriksson. Physical Review Letter 97 (2006) 164501.
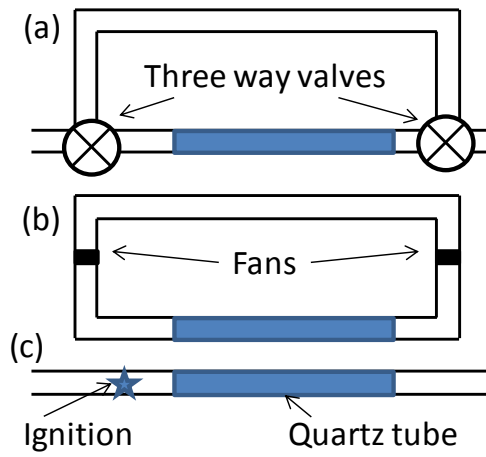
Figure captions

Figure 1. A schematic of the experimental configuration: (a) whole rig, (b) in mixing configuration and (c) in ignition configuration. Tube length 1200 mm, ignition 210 mm from the left hand side

Figure 2. Sample illustrations of: (a) typical single frame $(B/G) \in P(i,j)$ histogram at ϕ = 1.30; and (b) the computed Gaussian distribution at considered ϕ conditions

Figure 3. Calculated μ_e values at different Φ along with error bar denoting the 99% *CI* range

Figure 4. Images of stable propane/air flames

Figure 5. A and B, Image sequences of a ϕ = 1.2 propane air flame recorded at 3000 fps. C and D Colour image sequences of a ϕ = 1.2 propane air flame recorded at 1000 fps post processed to give *B/G* ratio. The numbers in the images relate to the time from the camera trigger and are provided to aid the comparison

Figure 6. Leading edge parameters plotted against time (a) flame position, (b) flame front position after subtraction of the fft filtered flame position, (c) observed flame speed. These relate to the image sequences Fig. 4 A & B

Figure 7. B/G ratio and flame front position against time from beginning of recording. These relate to the image sequences Fig.4 C & D

Figure 1. A schematic of the experimental configuration: (a) whole rig, (b) in mixing configuration and (c) in ignition configuration. Tube length 1200 mm, ignition 210 mm from the left hand side.
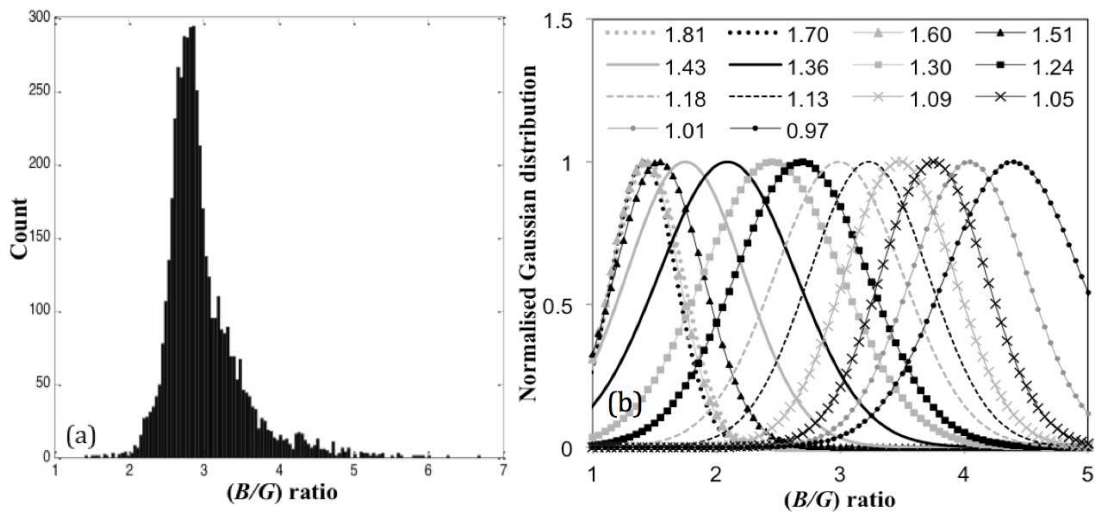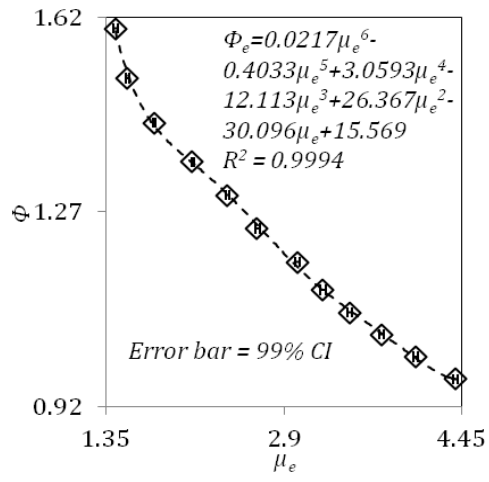

Figure 2. Sample illustrations of: (a) typical single frame $(\boldsymbol{B/G}) \in \boldsymbol{P}(\boldsymbol{i}, \boldsymbol{j})$ histogram at $\phi = 1.30$; and (b) the computed Gaussian distribution at considered ϕ conditions

Figure 3. Calculated μ_e values at different Φ along with error bar denoting the 99% *CI* range
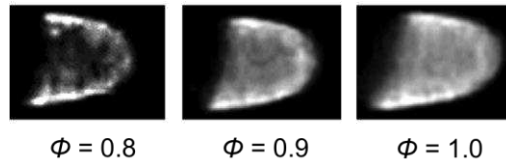
The equation shown in the figure:

$$\Phi_e = 0.0217\mu_e^6 - 0.4033\mu_e^5 + 3.0593\mu_e^4 - 12.113\mu_e^3 + 26.367\mu_e^2 - 30.096\mu_e + 15.569$$

$$R^2 = 0.9994$$

Error bar = 99% CI

$\Phi = 0.8$ $\Phi = 0.9$ $\Phi = 1.0$

Figure 4. Images of stable propane/air flames

Figure 5. A and B, Image sequences of a ϕ = 1.2 propane air flame recorded at 3000 fps. C and D Colour image sequences of a ϕ = 1.2 propane air flame recorded at 1000 fps post processed to give *B/G* ratio. The numbers in the images relate to the time from the camera trigger and are provided to aid the comparison
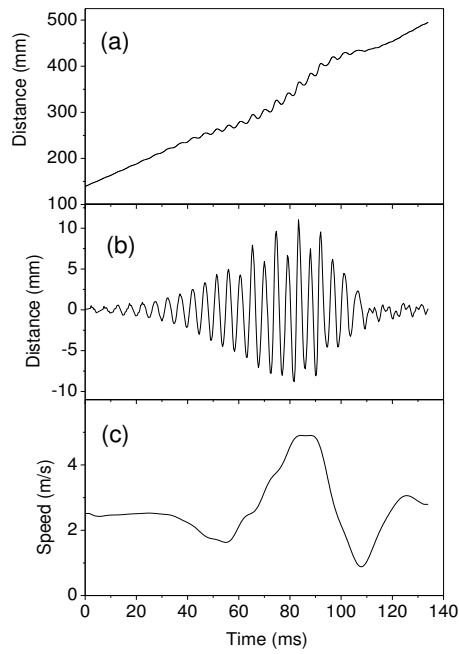
Figure 6. Leading edge parameters plotted against time (a) flame position, (b) flame front position after subtraction of the fft filtered flame position, (c) observed flame speed. These relate to the image sequences Fig. 4 A & B
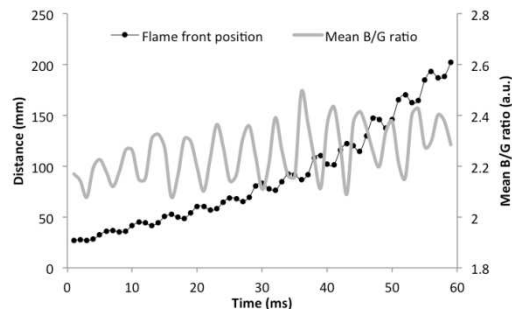

Figure 7. B/G ratio and flame front position against time from beginning of recording. These relate to the image sequences Fig.5 C & D